






Evolution of cross-frequency coupling between endogenous oscillations over the temporal cortex in very premature neonates

Bahar Saadatmehr¹, Mohammadreza Edalati ¹, Laura Routier^{1,2}, Mahdi Mahmoudzadeh ^{1,2}, Javad Safaie ³, Guy Kongolo^{1,4}, Ghida Ghostine^{1,4}, Fabrice Wallois ^{1,2}, Sahar Moghimi ^{1,2,*}

¹Inserm UMR1105, Groupe de Recherches sur l'Analyse Multimodale de la Fonction Cérébrale, CURS, Avenue Laennec, 80036 Amiens Cedex, France,

²Inserm UMR1105, EFSN Pédiatriques, CHU Amiens sud, Avenue Laennec, 80054 Amiens Cedex, France,

³Electrical Engineering Department, Ferdowsi University of Mashhad, 9177948974 Mashhad, Iran,

⁴Inserm UMR1105, NICU, CHU Amiens sud, Avenue Laennec, 80054 Amiens Cedex, France

*Corresponding author: Inserm UMR1105, Groupe de Recherches sur l'Analyse Multimodale de la Fonction Cérébrale, CURS, Avenue Laennec, 80036 Amiens Cedex, France. Email: sahar.moghimi@u-picardie.fr

Temporal theta activity in coalescence with slow-wave (TTA-SW) is one of the first neurobiomarkers of the neurodevelopment of perisylvian networks in the electroencephalography (EEG). Dynamic changes in the microstructure and activity within neural networks are reflected in the EEG. Slow oscillation slope can reflect synaptic strength, and cross-frequency coupling (CFC), associated with several putative functions in adults, can reflect neural communication. Here, we investigated the evolution of CFC, in terms of SW theta phase-amplitude coupling (PAC), during the course of very early development between 25 and 32 weeks of gestational age in 23 premature neonates. We used high-resolution EEG and dipole models as spatial filters to extract the source waveforms corresponding to TTA-SW. We also carried out nonlinear phase-dependent correlation measurements to examine whether the characteristics of the SW slopes are associated with TTA-SW coupling. We show that neurodevelopment leads to temporal accumulation of the SW theta PAC toward the trough of SW. Steepness of the negative going slope of SW determined the degree of this coupling. Systematic modulation of SW-TTA CFC during development is a signature of the complex development of local cortico-cortical perisylvian networks and distant thalamo-cortical neural circuits driving this nested activity over the perisylvian networks.

Key words: premature neonates; spontaneous neural activity; phase-amplitude coupling; electroencephalography.

Introduction

The layout of neuronal circuits responsible for processing sensory information is first established through molecular factors that guide axons to their target areas (Sanes and Yamagata 2009). The synaptic connections are then refined by spontaneous (Xu et al. 2011; Winnubst et al. 2015; Babola et al. 2018) and/or sensory-driven neural activity (Minlebaev et al. 2007; Colonnese et al. 2010; Colonnese and Khazipov 2010; Wess et al. 2017), preparing the developing neural networks for the processing of complex sensory information in a unique learning interaction with the environment (Mahmoudzadeh et al. 2013; Gervain 2018). Simultaneous dynamic integration and segregation of neural information at different timescales is a pivotal component of brain information coding. The characteristics of this multitimescale interaction of early oscillatory activities can be hallmarks of the dynamics of the underlying neural circuits, the disruption of which is dramatic for neurodevelopmental processes.

The ongoing developmental neural mechanisms in the third trimester of gestation (i.e. synaptogenesis, differentiation, migration, gyrification, and myelination) lead to electroencephalography (EEG) characteristics that change week by week (Dreyfus-Brisac et al. 1955; Dreyfus-Brisac 1962; Vecchierini et al. 2003; André et al. 2010). This period is also marked by the appearance of several transient waveforms with distinct spatiotemporal and spectral characteristics (Pavlidis et al. 2017; Bourel-Ponchel et al. 2021; Wallois et al. 2021). Some of these waveforms that are studied as biomarkers of normal neurodevelopment in clinic, display hierarchically nested oscillatory activities, consisting of a slow wave (SW) within which more rapid activities are nested; these include the theta temporal activities that coalesce with a SW (TTA-SW), localized and diffused delta brushes, and diffused slow activity transients (Vanhatalo et al. 2005; Kaminska et al. 2017; Routier et al. 2017; Moghimi et al. 2020).

Received: November 15, 2021. Revised: January 28, 2022. Accepted: January 29, 2022

© The Author(s) 2022. Published by Oxford University Press. All rights reserved. For permissions, please e-mail: journals.permissions@oup.com

This is an Open Access article distributed under the terms of the Creative Commons Attribution-NonCommercial License (<https://creativecommons.org/licenses/by-nc/4.0/>), which permits non-commercial re-use, distribution, and reproduction in any medium, provided the original work is properly cited. For commercial re-use, please contact journals.permissions@oup.com

TTA-SW can be recorded as early as 24 weeks of gestational age (wGA), with a peak of occurrence at approximately 27–28 wGA, and later disappearance at 33–34 wGA (Wallois et al. 2020). This is a transitional period during which thalamic afferents that were waiting in the subplate are relocated to layer IV (Kostović and Judaš 2010; Dubois et al. 2015), providing the cortical plate with the first inputs from the outside world. Before 28 wGA, the probability of occurrence of TTA-SW is not modified by auditory stimuli (Routier et al. 2017; Moghimi et al. 2020). The source of TTA-SW is located in the area of the planum temporal (Routier et al. 2017). The occurrence of TTA-SW increases the connectivity over the perisylvian network (Adebimpe et al. 2019). Overall, these features suggest that such nonsensory driven activity may participate in the functional wiring of the perisylvian auditory network. Analyzing TTA-SW provides a unique opportunity to investigate the early functional development of the perisylvian area, which is known to be involved in auditory processing, language, and communication (Friederici 2002).

In preterm neonates (24–27 wGA), we have demonstrated a precise temporal relationship, in terms of cross-frequency coupling (CFC), between slow delta waves and temporal theta activity such that the amplitude of TTA is orchestrated by the phase of the SW (phase-amplitude coupling, PAC) (Moghimi et al. 2020). CFC is a characteristic of intrinsic spontaneous oscillatory activity, which is believed to enhance combinatorial opportunities for encoding (Fell and Axmacher 2011; Rasch and Born 2013; Dehnavi et al. 2021) and synaptic plasticity (Buzsáki and Draguhn 2004; Bergmann and Born 2018; Salimpour and Anderson 2019; Peyrache and Seibt 2020).

Postmortem histological data show that the third trimester of gestation is marked by the rapid and dynamic evolution of thalamo-cortical and cortico-cortical neural circuits, presence of transient circuitries and maturation of permanent circuitries constructing the local and global brain networks (Kostović et al. 2021). Neuronal migration, as well as synaptogenesis, occurs during the last trimester of gestation (Kostović et al. 2018). The number of synapses in the subplate is high and its size continues to increase until 33 wGA. The first synapses appear in the cortical plate at approximately 26 wGA. At approximately 28 wGA, the thalamic afferents are relocated to the cortical plate (Dubois et al. 2015; Kostović et al. 2021). This allows phoneme and voice discrimination from 28 wGA onward (Mahmoudzadeh et al. 2013). This assumes that the previous steps (subtended by genetic fingerprints and/or spontaneous electrical activities) have functionally and structurally prepared the cortical auditory network in the perisylvian area, independently of exogenous sensory information.

Here, we searched for the signatures of neurodevelopment in the characteristics of this very early neurobiomarker, TTA-SW, which may shed light on the dynamics of the underlying neural circuits during this transitional period at the beginning of the third trimester of gestation. We hypothesized that the pattern of the PAC

of the nested oscillations within TTA-SW is determined by the developing thalamo-cortical and cortico-cortical neural networks and therefore might evolve during the course of the third trimester of gestation, likely providing a signature for the normal development of neural circuits. We evaluated this hypothesis by capturing the dynamics underlying the evolution of PAC between SW and TTA between 25 and 32 wGA (the time window in which TTA-SW can be detected from EEG signals). The characteristics of the PAC were analyzed separately over the left and right cortices, since the TTA-SW events are usually localized either to the left or to the right hemisphere, and in addition, previous studies have described an early structural asymmetry over the perisylvian areas (Dubois et al. 2007; Leroy et al. 2011). We used high-resolution EEG and dipole models as spatial filters to extract the source waveforms at the left and right temporal cortices (the neural source of TTA-SW) in preterm neonates. Finally, we used nonlinear phase-dependent correlation measures to examine whether the characteristics of the SW slopes are associated with TTA-SW coupling.

Materials and methods

Subjects

This study included 26 premature newborns, that were not included in our previous low-resolution EEG study (Moghimi et al. 2020) (Supplementary Table S1, gestational age: 25–32 wGA) in the neonatal intensive care unit of Amiens University Hospital (Amiens, France). All infants had appropriate birth weight, size, and head circumference for their term age (10th centile, Fenton and Kim 2013), an APGAR score > 5 at 5 min, and normal auditory and clinical neurological assessments. None were considered to be at risk of brain damage. In particular, the results of a neurological examination at the time of the recordings had to correspond to those of the corrected gestational age, with no history of abnormal movements. The gestational age (estimated from the date of the mother's last period and ultrasound measurements during pregnancy) corresponded to the degree of brain maturation (evaluated by EEG). The standard EEG had to be normal. The EEG evaluation in the follow up at the time they left the NICU had to be normal according to the EEG monitoring guideline of the French Society of Clinical Neuroscience for the very young premature. The other noninclusion criteria were a corrected age other than 25–32 wGA, the presence of neurological damage (such as intraventricular hemorrhage grades II, III, and IV or parenchymal malformation), intrauterine growth retardation, sepsis, and suspected necrotizing enterocolitis. The exclusion criterion were an abnormal interpretation of the high-resolution EEG, and the short duration of remaining data after preprocessing. The subjects were then divided into three groups (25–27 wGA: $n = 9$, 28–29 wGA: $n = 6$, and 30–32 wGA: $n = 11$) according to their age at the time of recording. One or both parents were informed about the study and provided their

written informed consent for the study and the use of photographic materials. The local ethics committee (CPP Ouest I) approved the study (ID-RCB: 2021-A02556-35).

EEG recordings

The HR-EEG was recorded in an incubator, while the premature neonates were asleep, using 64 Ag/AgCl surface electrodes and a sampling rate of 2000 Hz, amplified by a SynAmps RT 64-channel EEG/EP system (Compumedics Neuroscan) with a bandwidth from DC to 400 Hz. Impedances were kept below 5 k Ω . Because of rapid brain growth at this age, 3 caps were used to cover the normal range of head circumferences during this period. The electrocardiogram, deltoid electromyogram, and oxygen saturation level were also monitored. The EEG session was video-recorded.

EEG preprocessing

The EEG recordings were analyzed with MATLAB software (The MathWorks, Inc., Natick, MA) using FieldTrip (Oostenveld et al. 2011), EEGLAB (Delorme and Makeig 2004), and custom MATLAB functions and codes. First, for each subject, noisy channels were selected through visual inspection, and interpolated using the neighboring electrodes. Electrocardiography, ocular, and muscle artifacts were removed by independent component analysis using the EEGLAB toolbox. The EEG signals were then preprocessed using an automated artifact rejection algorithm. The samples were z-scored for each participant and electrode location using the mean \pm SD of the absolute amplitude after applying a 0.1–20 Hz 2-pass finite impulse response bandpass filter (order: 3 cycles of the low-frequency cut-off). A sample was recognized as an artifact if the z-score exceeded a value of 6. The 3-s segments preceding and following the artifact were marked and discarded from further analysis.

Modeling dipole waveforms of the temporal cortex

We employed a dipole source model (using FieldTrip) as a spatial filter to extract the EEG signals generated from left and right temporal cortices. This was performed using our neonatal finite element head model (detailed characteristics can be found in (Azizollahi et al. 2020)), which consists of 6 compartments: white and gray matter, cerebrospinal fluid, the fontanels, skull, and scalp. We were primarily interested in the activity over the planum temporale, based on our previous study, which located the source of TTA-SW over this area (Routier et al. 2017). Therefore, we analyzed the EEG signals in source space, rather than from surface electrodes (Fig. 1), by extracting the oscillatory signals generated from the left and right temporal cortices while attenuating signals generated from other brain regions. The dipole approach is a linear weighting of all surface electrodes that emphasizes the neural activity over the region of interest. The location of cortical sources, namely the left and right planum temporale, were specified by two experts (F.W. and

L.R.) using an magnetic resonance imaging (MRI) of a preterm neonate of 32 wGA (Ghadimi et al. 2016). Using the dipole model, the preprocessed 64-channel EEG was projected into source-space EEG for further analyses.

Detection of SW and TTA events

SWs and TTA were detected separately for each subject over the left and right source signals using the algorithms developed in our previous publication (Moghimani et al. 2020). The detection techniques were adapted from those previously used to detect sleep oscillations (namely slow oscillations [SOs] and spindles; Staresina et al. 2015; Mak-McCully et al. 2017; Gonzalez et al. 2018) and then adjusted to match the characteristics of the SWs and TTA observed here. Automated TTA-SW detection was verified by the manual detection of events among randomly sampled raw data by experienced clinical neurophysiologists (F.W. and L.R.). A sample event is presented in Figure 2.

For SW detection, data were first filtered between 0.1 and 2.5 Hz using a 2-pass finite impulse response band-pass filter (order: 3 cycles of the low-frequency cut-off). Next, all successive positive to negative zero-crossings in the filtered signal were identified. The event duration was defined as the time between the 2 zero-crossings. Events that met the SW duration criteria (a minimum of 1 s and a maximum of 2.8 s on each half-wave before and after the negative to positive zero-crossing, 0.1–2.5 Hz) were considered for the next step. The event amplitude was defined as the trough-to-peak amplitude. Events that also met the SW amplitude criterion (\geq 80th percentile of the candidate SW amplitudes), the SW peak amplitude criterion (\geq 75th percentile of the candidate SW peak amplitudes), and the SW trough amplitude criterion (\geq 75th percentile of the candidate SW trough amplitudes) were considered to be SWs. For all events, artifact-free epochs (–6 to +6 s, time-locked to the SW trough in the filtered signal) were extracted from the raw signal.

For TTA detection, the data were first filtered between 4 and 7.5 Hz using a 2-pass finite impulse response band-pass filter (order: 3 cycles of the low-frequency cut-off). Next, the RMS of the filtered signal was computed using a moving average window of 500 ms, and a TTA amplitude threshold corresponding to the 95th percentile of the RMS values was applied. A TTA event was detected if the signal exceeded this threshold for more than 0.5 s but less than 1.6 s. Artifact-free epochs (–6 to 6 s) centered on the TTA trough in the filtered signal were extracted from the unfiltered signal for further analysis.

An event was marked as TTA-SW if the largest trough of the TTA occurred between the first positive to negative zero-crossing and peak amplitude of the SW event.

Time–frequency analysis

We performed time–frequency representation (TFR) analysis to test the nesting hypothesis of SW and TTA by searching for power modulation during such

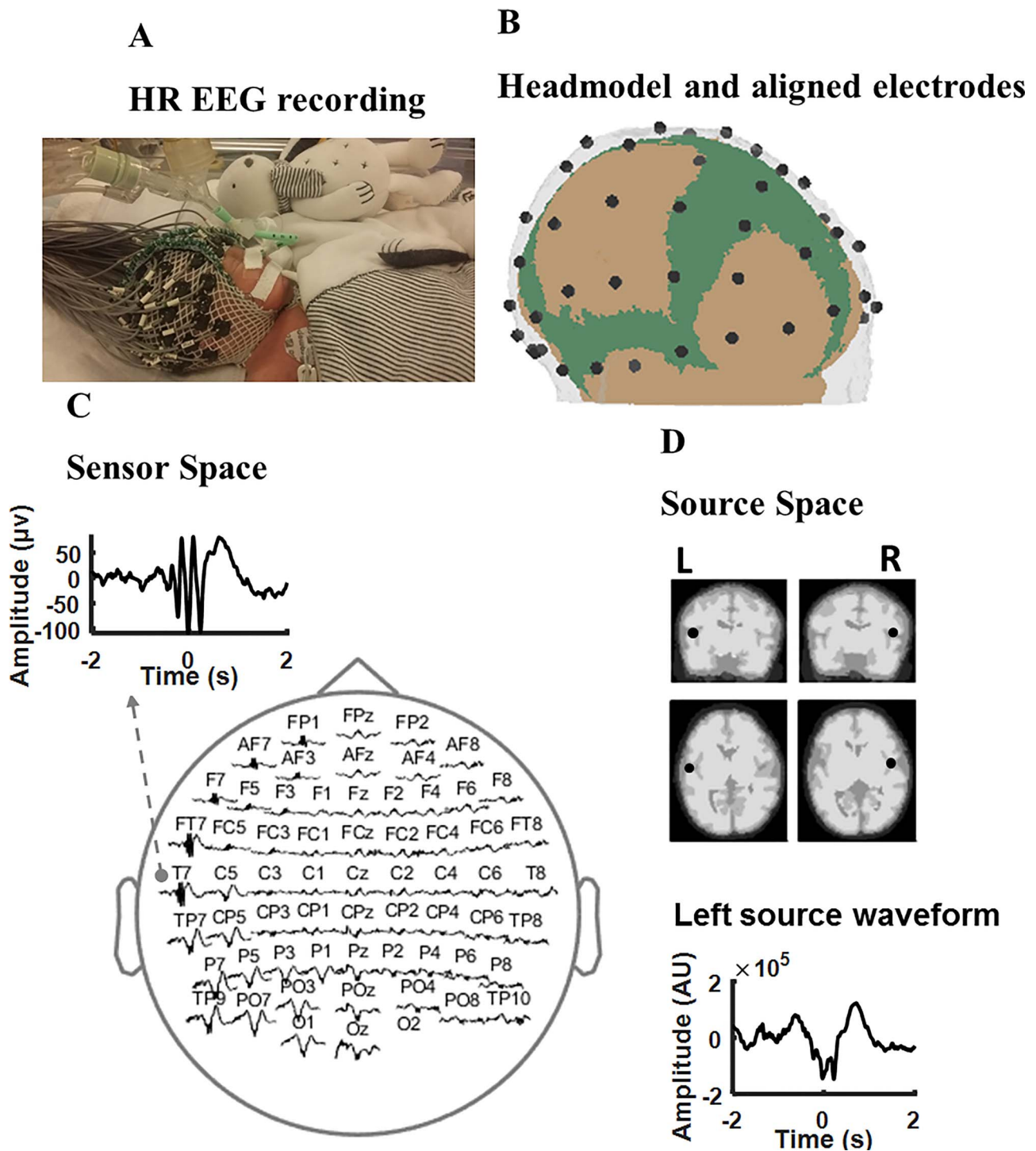


Fig. 1. High-resolution EEG recording, source localization, and event detection. (A) High resolution EEG recording of a preterm neonate at 28 wGA. (B) Electrode localization with the premature head model showing the skull, scalp, and fontanelles. (C) Distribution of a sample TTA-SW event over the electrodes. (D) Localization of the left and right temporal poles over an MRI of a preterm neonate, in addition to a source waveform for the event shown in (C) over the left temporal pole.

events. This was carried out over both the left and right temporal cortices and for each age group separately. The TFRs were computed per SW event (using the FieldTrip toolbox) for frequencies between 0.5 and 20 Hz, in steps of 0.05 Hz, using a sliding Hanning tapered window with a frequency-dependent length comprising a full number of cycles (always at least two). For

group-level statistics, 2-tailed paired-sample *t* tests were used to check for significant perievent power changes relative to the pre-event baseline (−2.5 to −1.2 s). The cluster-based permutation procedure implemented in the FieldTrip toolbox was used to correct for multiple comparisons (SW-triggered: −1.5 to +1.5 s × 0.5–20 Hz) (Oostenveld et al. 2011). The initial threshold for cluster

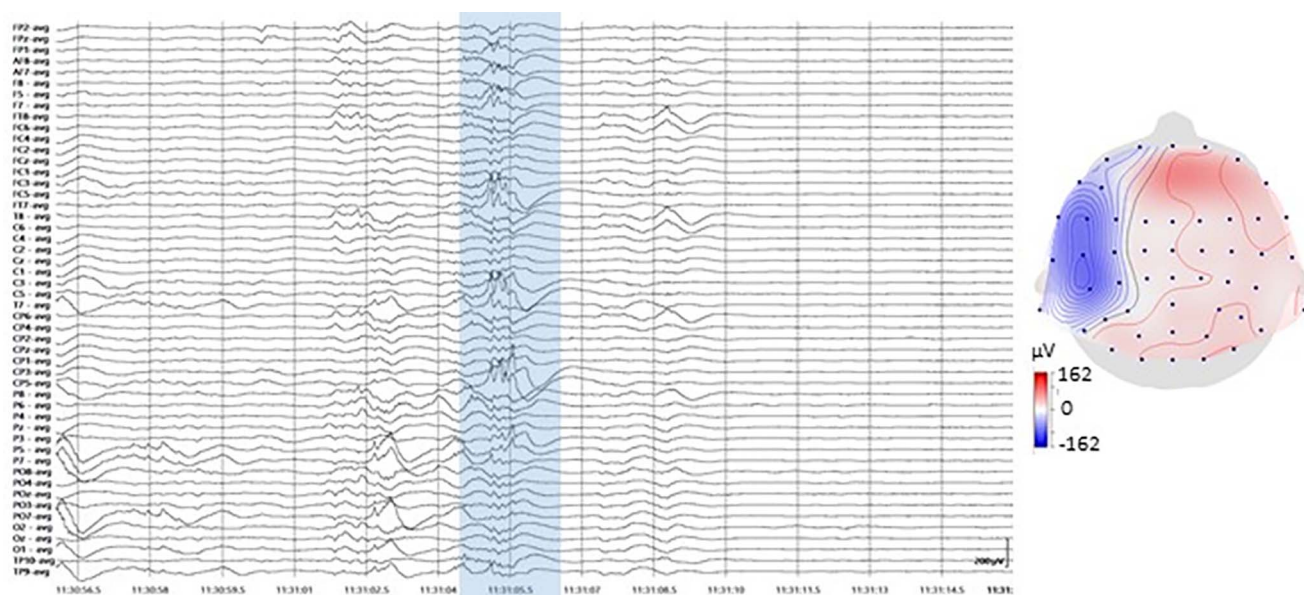


Fig. 2. Sample TTA-SW event recorded at 28 wGA (left), along with its topographical distribution (right). The topography corresponds to the largest trough of TTA.

definition was set to $P < 0.01$. Finally, the final significance threshold for summed t values within clusters was set to $P < 0.05$.

Phase-amplitude coupling analysis

The preferred phase of coupling (phase-amplitude coupling, PAC) between the phase of low-frequency (SW, modulating) and the amplitude of high-frequency (TTA, modulated) oscillations was extracted by separately filtering the source EEG signals in the frequency range corresponding to SW (0.5–2.5 Hz, 2-pass FIR bandpass filter, order = 3 cycles of the low cut-off frequency) and TTA (4–7.5 Hz, 2-pass FIR bandpass filter, order = 3 cycles of the low cut-off frequency). To avoid edge effects, we conducted 6-s zero-padding to each side of the ± 2 s long signal, with zero set to the trough of the SWs before filtering. Phase values were calculated for all samples of each extracted SW and the corresponding TA amplitude variations using Hilbert transform. TA power time series were created using TFR bins averaged across the respective frequencies (4–7.5 Hz) and up sampled to the sampling frequency of 512 Hz. The synchronization index (SI) was then computed between the 2 phase-value time series for each event epoch and channel. SI is a complex number, the radius of which indicates the strength of locking between SW and TA power fluctuations and the angle represents the “preferred phase” of synchronization (Staresina et al. 2015; Gonzalez et al. 2018), in other words, the phase of SW at which the power of TA is maximal across time.

$$SI = \frac{1}{N} \sum_{t=1}^N e^{j|\varphi_l(t) - \varphi_u(t)|}$$

where N is the number of samples, $\varphi_u(t)$ is the phase value of the fluctuations in TA power time series at

sample t , and $\varphi_l(t)$ is the phase value of SW time series at sample t (Cohen 2008). The synchronization index was calculated over the interval -1 to $+1$ s around the SW trough. Complex averaging was then performed, first for events for each subject individually and then for the subject belonging to the same age group.

SW slope calculation

The SW slope was calculated from EEG source signals filtered in the frequency range of 0.2–3.5 Hz. SW slopes during negative-going and positive-going wave transitions (Fig. 3B, right, and Supplementary Fig. S1) were determined as the ratio between the absolute value of the SW trough, corresponding to the peak of the negative SW half-wave, and the time interval from the previous and to the next zero crossing (Riedner et al. 2007; Dehnavi et al. 2021).

Statistical analysis

MATLAB (R2017b) was used for all statistical analyses. Unbalanced mixed model analyses of variance (ANOVA) with a within-subject factor hemisphere and a between subject factor age were performed to study the changes in TTA-SW density and SW slope. This was followed by 1-way ANOVA over each hemisphere separately to address the impact of age on density and slope changes.

All SI-related analyses were conducted using MATLAB CircStat toolbox (Berens 2009). We used the basic Rayleigh test to verify the circular nonuniformity of SI direction (at the individual level). The subjects for whom the null hypothesis could not be rejected were removed from further analyses. We used the Watson-Williams test (circular ANOVA equivalent) to study the modulation of SI direction by age. However, as there are no repeated measures or mixed-model statistical tests for circular

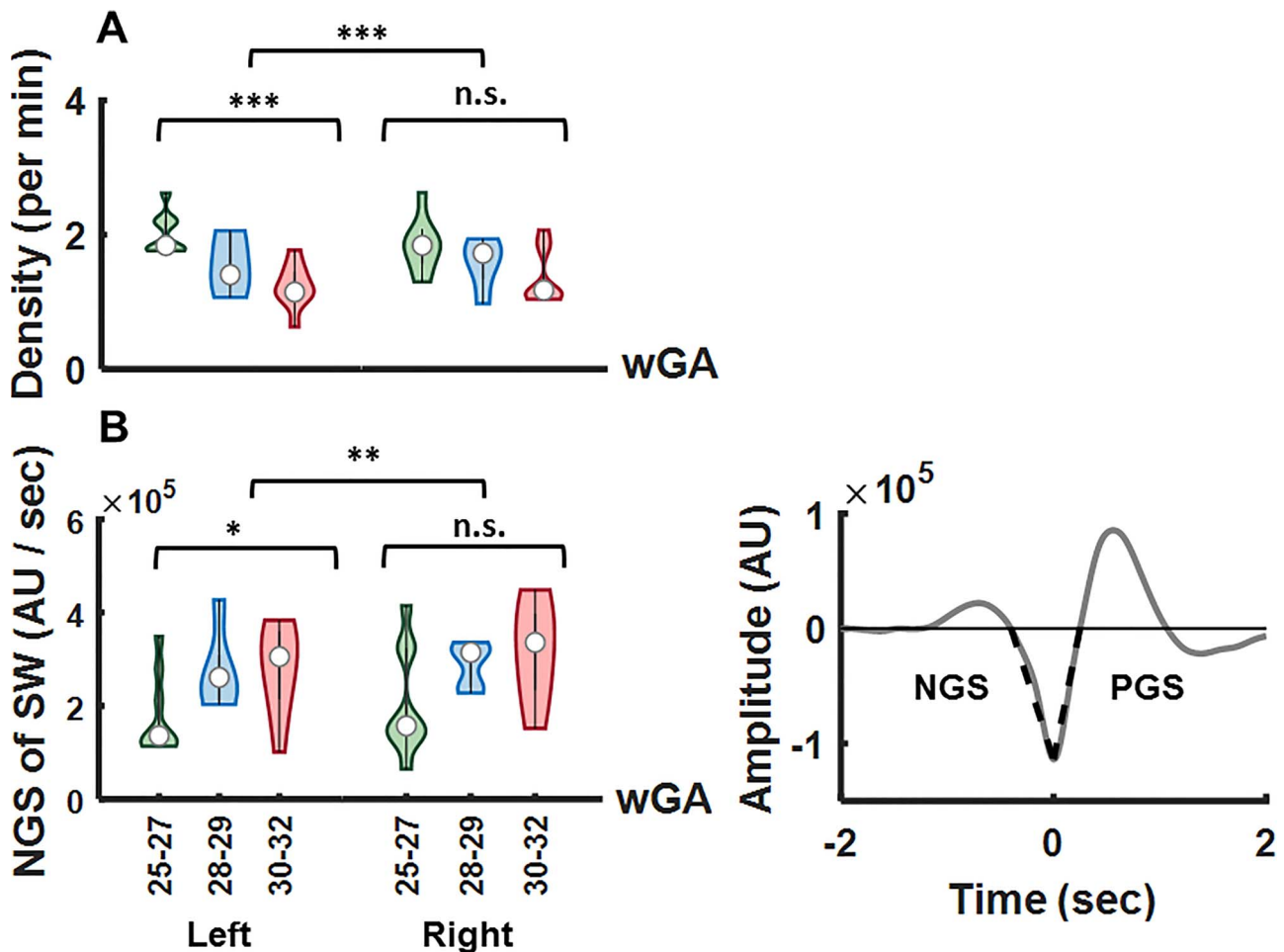


Fig. 3. (A) TTA-SW density decreased with age, as verified by a significant main effect of age ($F=21.41$, $P < 0.001$). The difference in density was significant between the left and right cortices ($F=191.83$, $P < 0.001$). A follow-up 1-way ANOVA with factor age revealed a significant effect of age over the left temporal cortex ($F=11.95$, $P < 0.001$), and a nonsignificant effect of age over the right temporal cortex ($F=2.96$, $P=0.075$). (B) The definition of the negative-going slope (NGS) and the positive-going slope (PGS) used for statistical analysis are shown on an exemplary SW event (right). The NGS of the SW increased significantly with age ($F=6.78$, $P < 0.05$). There was a significant difference between the NGS slope values corresponding to the 2 hemispheres ($F=10.17$, $P < 0.01$). A follow-up 1-way ANOVA with factor age revealed a significant effect of age over the left temporal cortex ($F=3.69$, $P < 0.05$), and a nonsignificant effect of age over the right temporal cortex ($F=2.77$, $P=0.09$).

data, we performed the Watson-Williams test separately for the left and right hemispheres, with age as the factor of interest. The circular-linear correlation was calculated to investigate the correlation between the SW slope and the preferred phase of coupling.

Results

We sought to demonstrate the evolution of cross-frequency interactions between neural oscillations as a signature of neurodevelopmental dynamics in the temporal cortex. We analyzed HR EEGs of preterm neonates (of 41.46 ± 13.45 min) in the source space between 25 and 32 wGA divided into 3 age groups: 25–27 wGA (26.33 ± 0.71 , $n=9$), 28–29 wGA (28.4 ± 0.55 , $n=5$), and 30–32 wGA (30.22 ± 0.67 , $n=9$); 2 subjects from the third age group and 1 from the second age group were discarded because the duration of the remaining data after preprocessing was short (2 subjects) and, in addition, the null hypothesis concerning the uniform

distribution of phases could not be rejected. We targeted the TTA and SW events over the bilateral temporal poles and tested whether the systematic modulation of the amplitude of theta oscillations by SW (i.e. the preferred phase of SW-TTA coupling) demonstrates a specific trend during development.

Signatures of TTA-SW during development

Our automated event detection algorithm yielded an average of 190.60 ± 65.63 SWs and 119.65 ± 32.23 TTAs per infant over the left temporal cortex and an average of 194.26 ± 64.18 SWs and 122.69 ± 35.81 TTAs per infant over the right temporal cortex. The mean event densities were 4.58 ± 0.31 per min for SWs and 2.95 ± 0.31 per min for TTAs over the left temporal cortex and 4.62 ± 0.30 per min for SWs and 2.97 ± 0.33 per min for TTAs over the right temporal cortex. The conventional measures of the events per age group are given in Table 1.

The density of the TTA-SW events decreased with age over both hemispheres, as shown by a significant main

Table 1. Conventional measures of the events per age group.

Infant n°	Duration (min)	SW density (per min)		TTA density (per min)		TTA-SW density (per min)	
		Left hemisphere	Right hemisphere	Left hemisphere	Right hemisphere	Left hemisphere	Right hemisphere
1	17.55	4.78	4.78	3.07	3.19	1.76	1.42
2	33.97	4.68	4.65	3.14	3.06	2.61	2.64
3	47.86	5.03	4.80	3.15	3.15	1.81	1.85
4	44.38	4.95	4.93	3.06	3.04	1.77	1.91
5	56.70	4.14	4.16	2.39	2.39	2.15	2.09
6	54.35	4.26	4.39	2.26	2.22	1.83	1.85
7	60	5.13	4.86	2.95	2.88	2.21	1.88
8	40.44	4.17	4.20	3.06	2.59	2.22	1.31
9	51.12	5.12	5.10	2.79	2.65	1.76	1.64
10	31.10	4.75	4.79	3.05	3.18	1.28	1.47
11	70.59	4.57	4.57	2.37	2.50	1.99	1.95
12	44.11	4.91	5.08	2.83	2.68	1.40	1.79
13	38.36	4.37	4.26	2.91	3.20	2.05	0.98
14	32.75	4.54	4.94	2.96	3.26	1.06	1.74
15	32.29	4.39	4.83	3.22	3.46	1.30	1.91
16	40.54	4.56	4.09	3.08	3.18	1.52	1.18
17	46.82	4.59	4.46	2.81	2.90	1.08	1.06
18	29.25	4.44	4.37	3.11	3.21	1.09	1.19
19	60.95	4.59	4.74	2.88	2.88	1.14	1.05
20	39.75	4.17	4.25	2.64	2.86	0.62	1.15
21	14.76	4.40	4.60	3.31	2.91	1.42	1.08
22	25.88	4.17	4.75	3.55	3.47	1.12	2.08
23	40.14	4.43	4.63	3.23	3.31	1.76	1.79

effect of age in an unbalanced mixed model ANOVA with the within-subject factor hemisphere and the between subject factor age ($F=21.41$, $P < 0.001$) (Fig. 3A). The effect of hemisphere ($F=191.83$, $P < 0.001$) and the interaction between the 2 factors ($F=15.46$, $P < 0.001$) were significant, demonstrating a stronger reduction in the density of events over the left temporal cortex than over the right temporal cortex. A follow-up 1-way ANOVA with the factor age showed a significant effect of age over the left temporal cortex ($F=11.95$, $P < 0.001$), and a nonsignificant effect of age over the right temporal cortex ($F=2.96$, $P=0.075$).

The negative-going SW slope increased from 25 to 32 wGA (Fig. 3B), leading to a significant main effect of age ($F=6.78$, $P < 0.05$). The interaction age \times hemisphere ($F=6.49$, $P < 0.05$) and the main effect of hemisphere ($F=10.17$, $P < 0.01$) were also significant, due to larger slopes over the right temporal cortex than over the left temporal cortex. A follow-up 1-way ANOVA with the factor age revealed a significant effect of age over the left ($F=3.69$, $P < 0.05$), and a nonsignificant effect of age over the right temporal cortex ($F=2.77$, $P=0.09$) temporal cortex. We did not find any significant effect for the positive-going slope of the SW for either hemisphere.

Temporal cortex maturation affects SW-TTA coupling

We first assessed in which phase of the SW TTA preferably occurs and then how development affects the preferred phase of coupling. First, perievent TFR time-locked to the SW trough (Fig. 4A and Supplementary Fig. S2A)

showed systematic power modulation of theta oscillations by SWs for all 3 age groups; the theta oscillations peaked around the SW trough: proceeding the SW trough (zoomed in from -0.4 to 0.4 s and on 3–20 Hz to highlight the nesting of TTA power in the SW trough). After thresholding, a significant cluster emerged around the SW trough for all 3 age groups ($P < 0.01$, corrected), relative to the pre-event baseline interval of -2.5 to -1.2 s, replicating our previous results in preterm neonates of 24–27 wGA (Moghimi et al. 2020). After showing that TTAs are locked to the SW trough, we addressed the impact of neurodevelopment on the modulation of the preferred phase of coupling. To this end, we first examined the general structure of the detected TTAs. The source waveforms over the temporal cortices were filtered (0.1–20 Hz) and averaged time-locked to the largest trough of all the detected TTAs. This analysis showed clear oscillations within the theta range riding on SWs, particularly nested around the SW trough (with its largest trough located after the SW trough, Fig. 4A and Supplementary Fig. S2A). The distance between the 2 troughs became smaller with neurodevelopment.

The PAC analysis (assessing the preferred modulation phase of TTA power by the SW) highlighted the temporal accumulation of the coupling toward the SW trough with age. Specifically, the average preferred phase of coupling changed from -130.92° for 25–27 wGA to -139.60° for 28–29 wGA and then to -146.79° for 30–32 wGA over the left temporal cortex, and changed from -130.24° for 25–27 wGA to -136.94° for 28–29 wGA, and then to -141.77° for 30–32 wGA over the right temporal

Left Hemisphere

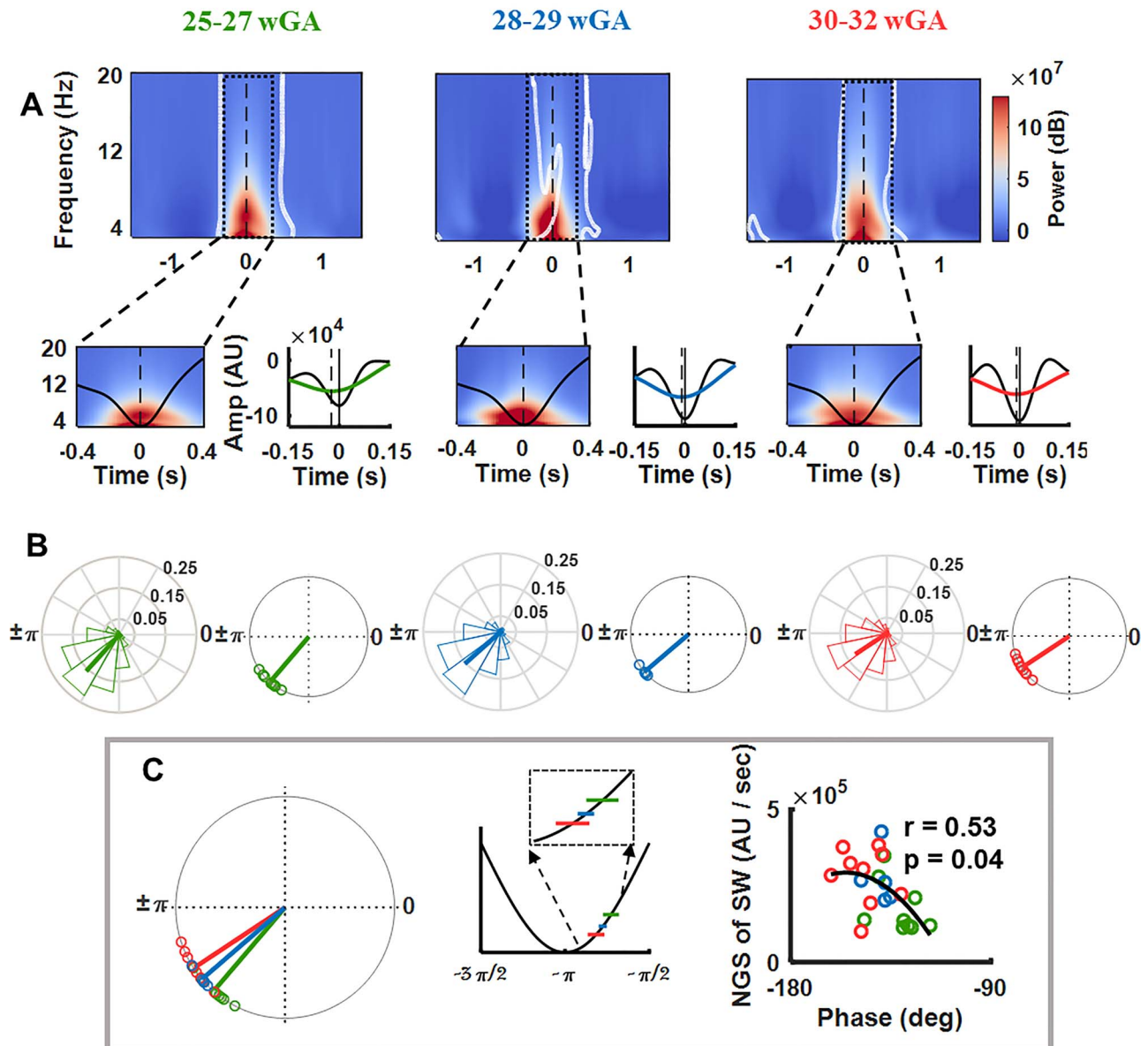


Fig. 4. Analysis of the evolution of SW TTA CFC during the course of development over the left temporal cortex. All results are presented for the 3 age groups: 25–27 wGA, 28–30 wGA, and 30–32 wGA. (A) Grand average of SW trough-locked TFR (zero at SW trough). The bottom panel shows the TFR zoomed in from -0.4 to 0.4 s to highlight the nesting of TTA power in the SW trough. On the right, the grand average 0.1 – 20 Hz EEG trace across neonates, aligned to the largest TTA trough (trough, time 0, zoomed over -0.15 to 0.15 s). (B) Normalized histogram of the preferred modulation phase of SW to TTA pooled over all newborns for each age group (left). The average phase is indicated by a bold line. The unit circle of preferred phases of SW to TTA modulation in each newborn for each age group (right). The Rayleigh test for nonuniformity was significant ($P < 0.001$) for all subjects. The preferred phases of SW to TTA modulation clustered at -130.92° for 25–27 wGA, at -139.6° for 28–29wGA, and at -146.79° for 30–32 wGA. (C) The effect of age on the preferred phase of coupling verified as significant ($F = 7.45$, $P < 0.01$). A positive circular-linear correlation was observed between the negative going slope of SW and SW-TTA coupling phase (circular-linear correlation, $r = 0.53$, $P < 0.05$). Each circle presents an individual with age being coded with color.

cortex, descending back over the positive-going slope of the SW and approaching the SW trough (Fig. 4B and Supplementary Fig. S2B). The impact of age on the preferred phase of coupling was significant over both the left ($F = 7.45$, $P < 0.01$) and right ($F = 5.48$, $P < 0.05$) temporal cortices as revealed by the Watson-Williams test. The Rayleigh test for nonuniformity was significant ($P < 0.001$) for all subjects. In addition, pooling all the subjects from the different age groups together resulted

in a robust positive correlation between the negative-going slope of the SW and SW-TTA coupling phase over the left hemisphere (circular-linear correlation, $r = 0.53$, $P < 0.05$; Fig. 4C), indicating that larger slope of SW leads to localization of theta oscillations toward the trough of SW. The same relationship was observed over the right temporal cortex; however, it did not verify as significant (circular-linear correlation, $r = 0.49$, $P = 0.06$; Supplementary Fig. S2C). The change in the strength

of coupling (defined as $1 - \text{circular variance}$) was not significant over the right hemisphere ($F = 0.46, P = 0.64$), whereas it decreased over the left hemisphere with age ($F = 5.30, P < 0.05$).

Discussion

The developmental period of 25–32 wGA corresponds to extremely preterm to very preterm. The organization of the circuitry goes through rapid changes during this period and thalamo-cortical and cortico-cortical neural circuits mature to shift the preterm brain from a sensory-expectant to a sensory-driven state (Kostović 2020). The appearance of TTA-SW is highly focalized to a small number of electrodes over the temporal and temporoparietal cortex, and despite the evolution of its characteristics (i.e. density and morphological characteristics) with gestational age, the source of this activity is always located adjacent to auditory and temporal junction areas. Here, we show that neurodevelopment leads to temporal accumulation of coupling toward the trough of SW, associated with an increase in the negative-going slope of SW. This modulation can be related to the development of thalamo-cortical pathways targeting the auditory cortex between 25 and 32 wGA, as well as the maturation of local cortico-cortical and subplate-cortical circuits over the auditory cortex. Modeling studies showed that the slope of SOs in EEG signals was positively correlated to the synaptic strength, and network synchronization in thalamo-cortical circuits (Esser et al. 2007), or that variations in synaptic strength of excitatory connections in a hippocampo-cortical network led to variations in the phase of coupling between nested oscillations (Azimi et al. 2021). Although these studies do not address the impact of neurodevelopment, we might assume that maturing circuitries can lead to similar impacts on the EEG manifestations. Given the rapidly ongoing neurodevelopmental phenomena (e.g. synaptogenesis and long/short distance connectivity) in the last trimester of gestation, the increase in synaptic strength and, as a result, improved synchronization of neuronal activity could explain the observed rise of the SW slope. SW likely reflects the activity of generators that provide a window of opportunity (due to greater excitability among postsynaptic neurons, which in turn synchronizes the synaptic input, Bergmann and Born 2018) for the emergence of synchronized theta oscillations, initiating in the descending part of the SW. In the framework of this hypothesis, the shift of the coupling phase toward the SW trough, accompanied by the increase in SW slope, reflects earlier synchronization of theta oscillations by the underlying maturing (and hence better synchronized) neural circuits. Collectively, our findings suggest that the modulation of the temporal SW and TTA coordination might index the development of local cortico-cortical and distant thalamo-cortical neural circuits over the temporal cortex. We have

previously suggested that appearance of this highly focalized and nonsensory-driven nested oscillation, before the relocation of thalamic afferents to the cortical plate, may indicate a role in the setup of the protomaps (Rakic 1988) over the auditory cortex. In this scenario, this index, defined as the evolution of PAC, can portrait the maturation of the circuits driving this phenomenon.

TTA-SW first appears before 26 wGA, at a time during which most of the synapses are concentrated in the subplate rather than in the cortical plate (Kostović et al. 2018). During this period, the reciprocal interactions between the subplate and cortical plate results in transient circuitries in which the subplate plays the role of an intermediary for thalamo-cortical and cortico-thalamic information processing. Progressively, the concert of interacting neural oscillations (both transient and permanent) becomes more complex, leading to hierarchical nesting of different oscillatory activities. Similar to other spontaneous neurobiomarkers of development, such as the delta brush in premature neonates (Kaminska et al. 2017) and spindle bursts in rodents (Luhmann and Khazipov 2018), TTA-SW cannot be detected after a certain stage of early neurodevelopment. However, while present, its nesting characteristics are modulated by the developing neural concert of the underlying networks in communication. In the rat barrel cortex, local smooth delta waves start to demonstrate nested high-frequency oscillations 2 days after birth (Khazipov and Milh 2018). The origin of these slow oscillations and that of the nested high-frequency oscillations are in the thalamus. In parallel, it has been suggested that thalamic input to the pyramidal cells in layer VI, as well as the subplate, may contribute to delta waves in human preterm neonates (Kostović and Judaš 2010). However, during this period of development, both the transient subplate circuitry and the permanent thalamo-cortical circuitry undergo rapid evolution (Kostović 2020). Therefore, a stronger conclusion concerning the role of developing local subplate/cortical networks or the long distance thalamo-cortical networks in the modulation of the temporal coordination of nested oscillations requires further studies in animal models.

We have performed the analyses separately over the two hemisphere (considering a factor of hemisphere in the analyses), to see if at this very early stage of development, the spontaneous nested oscillations over the temporal cortices favor an asymmetry between the 2 cortices. This strategy was chosen based on the evidence suggesting a different early developmental time-course for the left and right perisylvian cortical areas (Dubois et al. 2007; Leroy et al. 2011), along with an early asymmetry in the neural response to auditory stimulation as early as 28 wGA (Mahmoudzadeh et al. 2013). Although, in this study we found hemispheric differences in different parameters of interest including the slope, as well as the significant correlation between the phase of coupling and the SW slope, we cannot draw a conclusion favoring

an asymmetry in the developmental time course of TTA-SW characteristics. In order to be prudent, this issue has to be studied in a larger cohort.

Experimental results suggest impairment of temporal coordination between spontaneous oscillations during sleep (notably SO and spindles) due to aging (Helfrich et al. 2018), manifesting as a shift in the phase of SO-spindle coupling. In contrast, improved SO-spindle temporal coordination with brain maturation has been reported in terms of an increase in coupling strength (and not a variation in the phase of coupling) from childhood to adolescence (Hahn et al. 2020). In the current study, the strength of coupling decreased over the left temporal cortex and did not show a significant trend over the right temporal cortex. However, TTA-SW is a transient neurobiomarker and its density decreases with neurodevelopment (more pronounced over the left than right temporal cortex). The definition of the value of coupling strength depends on the circular deviation of the phase of coupling between individual events. As a result, a reduction in the density of events with age can have an impact on the calculated values for coupling strength. Therefore, changes in the strength of coupling have to be interpreted with caution.

TTA-SW constitutes one of the initial neurobiomarkers observed in premature neonates. Its localization over the temporal cortex suggests its possible role in the early development of perisylvian auditory networks. Systematic modulation of SW-TTA CFC in the course of development can be considered as a signature of the complex development of the underlying network. The monitoring of such dynamics in the coupling between TTA and SW may be helpful for the initial EEG follow-up of normal development in this at-risk population, the extremely preterm neonates. Future longitudinal studies may also consider a possible early predictive value, in which the absence of maturational dynamics in the coupling could indicate a poor prognosis for the development of perisylvian auditory functions.

Acknowledgments

The authors are grateful to the Amiens university hospital EEG technicians for data acquisition. We thank the parents and families who consented to take part in the study.

Supplementary material

Supplementary material is available at *Cerebral Cortex Journal* online.

Funding

This work has been supported by Agence Nationale de la Recherche (ANR 2015 CE MAIA), Cognitive Sciences and Technology Council (COGC) Iran (Neurobiom), and Eiffel Excellence scholarship (P729740-H).

Data Availability Statement

The datasets used during the current study, as well as the software and/or algorithms essential to the conclusions of this work are available from the corresponding author on reasonable request.

Conflict of interest statement. None declared.

References

- Adebimpe A, Routier L, Wallois F. Preterm modulation of connectivity by endogenous generators: the theta temporal activities in coalescence with slow waves. *Brain Topogr.* 2019;32(5):762–772. <https://doi.org/10.1007/s10548-019-00713-z>.
- André M, Lamblin MD, d'Allest AM, Curzi-Dascalova L, Moussalli-Salefranque F, Nguyen The Tich S, Vecchierini-Blineau MF, Wallois F, Walls-Esquivel E, Plouin P. Electroencephalography in premature and full-term infants. Developmental features and glossary. *Neurophysiologie Clinique/Clin Neurophysiol.* 2010;40(2):59–124. <https://doi.org/10.1016/j.neucli.2010.02.002>.
- Azimi A, Alizadeh Z, Ghorbani M. The essential role of hippocampocortical connections in temporal coordination of spindles and ripples. *NeuroImage.* 2021;243:118485. <https://doi.org/10.1016/j.neuroimage.2021.118485>.
- Azizollahi H, Aarabi A, Wallois F. Effect of structural complexities in head modeling on the accuracy of EEG source localization in neonates. *J Neural Eng.* 2020;17(5):056004. <https://doi.org/10.1088/1741-2552/abb994>.
- Babola TA, Li S, Gribizis A, Lee BJ, Issa JB, Wang HC, Crair MC, Bergles DE. Homeostatic control of spontaneous activity in the developing auditory system. *Neuron.* 2018;99(3):511–524.e5. <https://doi.org/10.1016/j.neuron.2018.07.004>.
- Berens P. CircStat: AMATLABToolbox for circular statistics. *J Stat Softw.* 2009;31(10):1–21. <https://doi.org/10.18637/jss.v031.i10>.
- Bergmann TO, Born J. Phase-amplitude coupling: a general mechanism for memory processing and synaptic plasticity? *Neuron.* 2018;97(1):10–13. <https://doi.org/10.1016/j.neuron.2017.12.023>.
- Bourel-Ponchel E, Gueden S, Hasaerts D, Héberlé C, Malfilâtre G, Mony L, Vignolo-Diard P, Lamblin MD. Normal EEG during the neonatal period: maturational aspects from premature to full-term newborns. *Neurophysiol Clin.* 2021;51(1):61–88. <https://doi.org/10.1016/j.neucli.2020.10.004>.
- Buzsáki G, Draguhn A. Neuronal oscillations in cortical networks. *Science.* 2004;304(5679):1926–1929. <https://doi.org/10.1126/science.1099745>.
- Cohen MX. Assessing transient cross-frequency coupling in EEG data. *J Neurosci Methods.* 2008;168(2):494–499. <https://doi.org/10.1016/j.jneumeth.2007.10.012>.
- Colonnese MT, Khazipov R. “Slow activity transients” in infant rat visual cortex: a spreading synchronous oscillation patterned by retinal waves. *J Neurosci.* 2010;30(12):4325–4337. <https://doi.org/10.1523/jneurosci.4995-09.2010>.
- Colonnese MT, Kaminska A, Minlebaev M, Milh M, Bloem B, Lescure S, Moriette G, Chiron C, Ben-Ari Y, Khazipov R. A conserved switch in sensory processing prepares developing neocortex for vision. *Neuron.* 2010;67(3):480–498. <https://doi.org/10.1016/j.neuron.2010.07.015>.
- Dehnavi F, Koo-Poeggel PC, Ghorbani M, Marshall L. Spontaneous slow oscillation—slow spindle features predict induced overnight memory retention. *Sleep.* 2021;44(10):1–12. <https://doi.org/10.1093/sleep/zsab127>.

- Delorme A, Makeig S. EEGLAB: an open source toolbox for analysis of single-trial EEG dynamics including independent component analysis. *J Neurosci Methods*. 2004;134(1):9–21. <https://doi.org/10.1016/j.jneumeth.2003.10.009>.
- Dreyfus-Brisac C. The electroencephalogram of the premature infant. *World Neurol*. 1962;3:5–15.
- Dreyfus-Brisac C, Samsondollfus D, Fischgold H. Cerebral electrical activity in premature and newborn infants. *La semaine des hopitaux: organe fonde par l'Association d'enseignement medical des hopitaux de Paris*. 1955;31(31/3):1783–1790.
- Dubois J, Benders M, Cachia A, Lazeyras F, Ha-Vinh Leuchter R, Sizonenko SV, Borradori-Tolsa C, Mangin JF, Huppi PS. Mapping the early cortical folding process in the preterm newborn brain. *Cereb Cortex*. 2007;18(6):1444–1454. <https://doi.org/10.1093/cercor/bhm180>.
- Dubois J, Kostovic I, Judas M. Development of structural and functional connectivity. *Brain Mapping*. 2015;2:423–437. <https://doi.org/10.1016/b978-0-12-397025-1.00360-2>.
- Esser SK, Hill SL, Tononi G. Sleep homeostasis and cortical synchronization: I. Modeling the effects of synaptic strength on sleep slow waves. *Sleep*. 2007;30(12):1617–1630. <https://doi.org/10.1093/sleep/30.12.1617>.
- Fell J, Axmacher N. The role of phase synchronization in memory processes. *Nat Rev Neurosci*. 2011;12(2):105–118. <https://doi.org/10.1038/nrn2979>.
- Fenton TR, Kim JH. A systematic review and meta-analysis to revise the Fenton growth chart for preterm infants. *BMC Pediatr*. 2013;13(1):1–13. <https://doi.org/10.1186/1471-2431-13-59>.
- Friederici AD. Towards a neural basis of auditory sentence processing. *Trends Cogn Sci*. 2002;6(2):78–84. [https://doi.org/10.1016/s1364-6613\(00\)01839-8](https://doi.org/10.1016/s1364-6613(00)01839-8).
- Gervain J. The role of prenatal experience in language development. *Curr Opin Behav Sci*. 2018;21:62–67. <https://doi.org/10.1016/j.cobeha.2018.02.004>.
- Ghadimi S, Abrishami Moghaddam H, Grebe R, Wallois F. Skull segmentation and reconstruction from newborn CT images using coupled level sets. *IEEE J Biomed Health Inform*. 2016;20(2):563–573. <https://doi.org/10.1109/jbhi.2015.2391991>.
- Gonzalez CE, Mak-McCully RA, Rosen BQ, Cash SS, Chauvel PY, Bastuji H, Rey M, Halgren E. Theta bursts precede, and spindles follow, cortical and thalamic downstates in human NREM sleep. *J Neurosci*. 2018;38(46):9989–10001. <https://doi.org/10.1523/jneurosci.0476-18.2018>.
- Hahn MA, Heib D, Schabus M, Hoedlmoser K, Helfrich RF. Slow oscillation-spindle coupling predicts enhanced memory formation from childhood to adolescence. *elife*. 2020;9:e53730, 1–20. <https://doi.org/10.7554/elife.53730>.
- Helfrich RF, Mander BA, Jagust WJ, Knight RT, Walker MP. Old brains come uncoupled in sleep: slow wave-spindle synchrony, brain atrophy, and forgetting. *Neuron*. 2018;97(1):221–230. <https://doi.org/10.1016/j.neuron.2017.11.020>.
- Kaminska A, Delattre V, Laschet J, Dubois J, Labidurie M, Duval A, Manresa A, Magny JF, Hovhannisyann S, Mokhtari M, et al. Cortical auditory-evoked responses in preterm neonates: revisited by spectral and temporal analyses. *Cereb Cortex*. 2017;28(10):3429–3444. <https://doi.org/10.1093/cercor/bhx206>.
- Khazipov R, Milh M. Early patterns of activity in the developing cortex: focus on the sensorimotor system. *Semin Cell Dev Biol*. 2018;76:120–129. <https://doi.org/10.1016/j.semcdb.2017.09.014>.
- Kostović I. The enigmatic fetal subplate compartment forms an early tangential cortical nexus and provides the framework for construction of cortical connectivity. *Prog Neurobiol*. 2020;194:101883. <https://doi.org/10.1016/j.pneurobio.2020.101883>.
- Kostović I, Judaš M. The development of the subplate and thalamocortical connections in the human foetal brain. *Acta Paediatr*. 2010;99(8):1119–1127. <https://doi.org/10.1111/j.1651-2227.2010.01811.x>.
- Kostović I, Išasegi IU, Krsnik E. Sublaminar organization of the human subplate: developmental changes in the distribution of neurons, glia, growing axons and extracellular matrix. *J Anat*. 2018;235(3):481–506. <https://doi.org/10.1111/joa.12920>.
- Kostović I, Radoš M, Kostović-Srzić M, Krsnik E. Fundamentals of the development of connectivity in the human fetal brain in late gestation: from 24 weeks gestational age to term. *J Neuropathol Exp Neurol*. 2021;80(5):393–414. <https://doi.org/10.1093/jnen/nlab024>.
- Leroy F, Glasel H, Dubois J, Hertz-Pannier L, Thirion B, Mangin JF, Dehaene-Lambertz G. Early maturation of the linguistic dorsal pathway in human infants. *J Neurosci*. 2011;31(4):1500–1506. <https://doi.org/10.1523/jneurosci.4141-10.2011>.
- Luhmann HJ, Khazipov R. Neuronal activity patterns in the developing barrel cortex. *Neuroscience*. 2018;368:256–267. <https://doi.org/10.1016/j.neuroscience.2017.05.025>.
- Mahmoudzadeh M, Dehaene-Lambertz G, Fournier M, Kongolo G, Goudjil S, Dubois J, Grebe R, Wallois F. Syllabic discrimination in premature human infants prior to complete formation of cortical layers. *Proc Natl Acad Sci*. 2013;110(12):4846–4851. <https://doi.org/10.1073/pnas.1212220110>.
- Mak-McCully RA, Rolland M, Sargsyan A, Gonzalez C, Magnin M, Chauvel P, Rey M, Bastuji H, Halgren E. Coordination of cortical and thalamic activity during non-REM sleep in humans. *Nat Commun*. 2017;8(1):1–11. <https://doi.org/10.1038/ncomms15499>.
- Minlebaev M, Ben-Ari Y, Khazipov R. Network mechanisms of spindle-burst oscillations in the neonatal rat barrel cortex in vivo. *J Neurophysiol*. 2007;97(1):692–700. <https://doi.org/10.1152/jn.00759.2006>.
- Moghim S, Shadkam A, Mahmoudzadeh M, Calipe O, Panzani M, Edalati M, Ghorbani M, Routier L, Wallois F. The intimate relationship between coalescent generators in very premature human newborn brains: quantifying the coupling of nested endogenous oscillations. *Hum Brain Mapp*. 2020;41(16):4691–4703. <https://doi.org/10.1002/hbm.25150>.
- Oostenveld R, Fries P, Maris E, Schoffelen JM. FieldTrip: open source software for advanced analysis of MEG, EEG, and invasive electrophysiological data. *Comput Intell Neurosci*. 2011;2011:1–9. <https://doi.org/10.1155/2011/156869>.
- Pavlidis E, Lloyd RO, Boylan GB. EEG - a valuable biomarker of brain injury in preterm infants. *Dev Neurosci*. 2017;39(1–4):23–35. <https://doi.org/10.1159/000456659>.
- Peyrache A, Seibt J. A mechanism for learning with sleep spindles. *Philos Trans R Soc B: Biol Sci*. 2020;375(1799):20190230. <https://doi.org/10.1098/rstb.2019.0230>.
- Rakic P. Specification of cerebral cortical areas. *Science*. 1988;241(4862):170–176. <https://doi.org/10.1126/science.3291116>.
- Rasch B, Born J. About sleep's role in memory. *Physiol Rev*. 2013;93(2):681–766. <https://doi.org/10.1152/physrev.00032.2012>.
- Riedner BA, Vyazovskiy VV, Huber R, Massimini M, Esser S, Murphy M, Tononi G. Sleep homeostasis and cortical synchronization: III. A high-density EEG study of sleep slow waves in humans. *Sleep*. 2007;30(12):1643–1657. <https://doi.org/10.1093/sleep/30.12.1643>.
- Routier L, Mahmoudzadeh M, Panzani M, Azizollahi H, Goudjil S, Kongolo G, Wallois F. Plasticity of neonatal neuronal networks in very premature infants: source localization of temporal theta activity, the first endogenous neural biomarker, in temporoparietal areas. *Hum Brain Mapp*. 2017;38(5):2345–2358. <https://doi.org/10.1002/hbm.23521>.

- Salimpour Y, Anderson WS. Cross-frequency coupling based neuromodulation for treating neurological disorders. *Front Neurosci*. 2019;13:125. <https://doi.org/10.3389/fnins.2019.00125>.
- Sanes JR, Yamagata M. Many paths to synaptic specificity. *Annu Rev Cell Dev Biol*. 2009;25(1):161–195. <https://doi.org/10.1146/annurev.cellbio.24.110707.175402>.
- Staresina BP, Bergmann TO, Bonnefond M, van der Meij R, Jensen O, Deuker L, Elger CE, Axmacher N, Fell J. Hierarchical nesting of slow oscillations, spindles and ripples in the human hippocampus during sleep. *Nat Neurosci*. 2015;18(11):1679–1686. <https://doi.org/10.1038/nn.4119>.
- Vanhatalo S, Palva JM, Andersson S, Rivera C, Voipio J, Kaila K. Slow endogenous activity transients and developmental expression of K⁺-Cl⁻-cotransporter 2 in the immature human cortex. *Eur J Neurosci*. 2005;22(11):2799–2804. <https://doi.org/10.1111/j.1460-9568.2005.04459.x>.
- Vecchierini MF, D'Allest AM, Verpillat P. EEG patterns in 10 extreme premature neonates with normal neurological outcome: qualitative and quantitative data. *Brain Dev*. 2003;25(5):330–337. [https://doi.org/10.1016/s0387-7604\(03\)00007-x](https://doi.org/10.1016/s0387-7604(03)00007-x).
- Wallois F, Routier L, Bourel-Ponchel E. Impact of prematurity on neurodevelopment. *Handb Clin Neurol*. 2020;173:341–375. <https://doi.org/10.1016/b978-0-444-64150-2.00026-5>.
- Wallois F, Routier L, Heberlé C, Mahmoudzadeh M, Bourel-Ponchel E, Moghimi S. Back to basics: the neuronal substrates and mechanisms that underlie the electroencephalogram in premature neonates. *Neurophysiol Clin*. 2021;51(1):5–33. <https://doi.org/10.1016/j.neucli.2020.10.006>.
- Wess JM, Isaiah A, Watkins PV, Kanold PO. Subplate neurons are the first cortical neurons to respond to sensory stimuli. *Proc Natl Acad Sci*. 2017;114(47):12602–12607. <https://doi.org/10.1073/pnas.1710793114>.
- Winnubst J, Cheyne J, Niculescu D, Lohmann C. Spontaneous activity drives local synaptic plasticity in vivo. *Neuron*. 2015;87(2):399–410. <https://doi.org/10.1016/j.neuron.2015.06.029>.
- Xu HP, Furman M, Mineur Y, Chen H, King S, Zenisek D, Zhou Z, Butts D, Tian N, Picciotto M, et al. An instructive role for patterned spontaneous retinal activity in mouse visual map development. *Neuron*. 2011;70(6):1115–1127. <https://doi.org/10.1016/j.neuron.2011.04.028>.